SSRG International Journal of Electronics and Communication Engineering
ISSN: 2348 – 8549 / https://doi.org/10.14445/23488549/IJECE-V9I4P101

Volume 9 Issue 4, 1-9, April 2022


*Original Article*

# Home Rehabilitation of Patients using Bioelectronics Nano-Medicine Devices and 65nm CMOS Embedded Electronics for Insulation to Avoid Coronavirus Infection

Hafez Fouad[1], Hesham Kamel[2]

[1] *Department of Microelectronics, Electronics Research Institute, Cairo, Egypt.*
[2] *Electronics and Communications Department, School of Engineering, Canadian higher Engineering Institute, CIC (Canadian International College), 6th October, Giza, Egypt.*

Received : 26 February 2022 Revised : 05 April 2022 Accepted : 15 April 2022 Published : 30 April 2022

***Abstract*** *- This paper aims to adopt nano-medicine devices with bionics (function like living organisms) in embedded systems (isolation) to allow health rehabilitation of patients at home to avoid infection with the Coronavirus. Measuring various patients' vital signals such as temperature, blood oxygen percentage, blood pressure, heartbeat, and glucose level (to pump insulin to the body to control the blood sugar level) are included in our objective. In this work, we developed a Class AB 65nm CMOS system that can be used as part of Medical IOT applications in Telemedicine and remote healthcare. Our proposed circuit has been designed and simulated using CADENCE Design Tools in TMSC 65nm CMOS technology to optimize the design and get the required specifications. This paper designed a 2.4 GHz Class AB CMOS PA with a CG driver stage followed by a CS power stage using the proposed method for WBAN applications. The simulation results showed that the proposed PA achieved a maximum PAE of 49.09% and had an average gain of 32.4 dB over the frequency of interest in Industrial, Scientific, and Medical (ISM) bands. Input Reflection Coefficient S11=-38.588 dB, Psat=15.6172 dBm Output referred compression point P1dB=11.784 dBm. The Physical layout of the proposed CMOS Class-AB Amplifier has been designed and optimized to a 0.085mm2 chip area.*

***Keywords*** *– Bioelectronics, Wearable and Implantable sensors, Power amplifier, Class AB, Embedded systems, Healthcare monitoring, nano-medicine, Coronavirus, Internet of Things IoT, 65nm CMOS, Energy harvest, Organic devices.*

## 1. Introduction

Telemedicine allows continuous monitoring of patient's health conditions, which could not be done quickly at hospitals due to the associated cost and limited places. Thus, telemedicine will help reduce the load at hospitals and medical centers, where patients' vital signs will be sent remotely to healthcare providers [1]. Energy harvesting is when ambient energy is captured and converted directly into electricity for supplying small and mid-sized devices, such as autonomous wireless sensor nodes, implanted medical devices, and consumers.

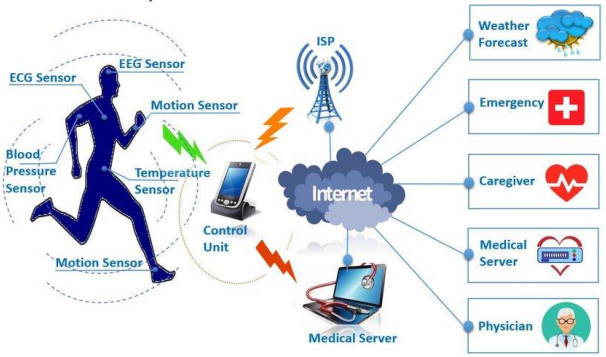


**Fig. 1 A wearable bioelectronics system monitors various vital signs and communicates wirelessly with different levels of healthcare providers [2]**


**Fig. 2 Powering techniques/ sources for implantable and wearable bioelectronics medical devices [3]**

Wearable and Implantable technologies contribute to transfer in the mobile health era to improve healthcare and health outcomes and provide real-time guidance on improved health management and tracking, Fig.3. reviews

biomedical applications of wearable and implantable medical devices and sensors, ranging from monitoring to preventing diseases, the materials used to fabricate these devices, and the standards for wireless medical devices and mobile applications. We conclude by discussing some technical challenges in wearable and implantable technology and possible solutions for overcoming these difficulties.

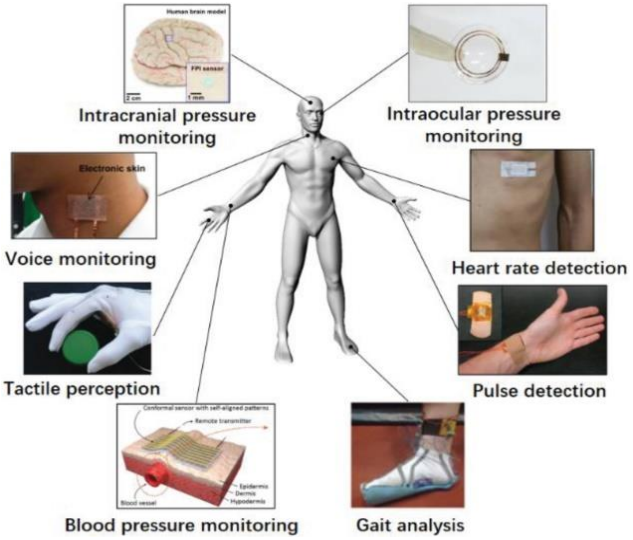


**Fig. 3 Examples of Implantable Bioelectronics Applications[4]**

## 2. Healthcare Facilities

### *2.1. Personal Medical Diagnostics and Monitoring*

They represent the greatest near-term application opportunity. This area includes multimodal (optical, chemical, electronic) single-molecule detection systems that detect low concentrations of molecules in dirty environments, such as blood. It also includes label-free detection using sensors that leverage semiconductor technology, ideally with single-molecule resolution. Fig.4 shows a personal medical diagnostic and monitoring system. Fig.5a, b shows Recognition of Daily human activities observation.

### *2.2. Implantable Medical Devices (IMD) and Prosthetics*

The second-highest-ranked research area was neural-electronic interfaces and prosthetics-related research that would enable reliable and robust implantable sensors and devices. A key issue in this area is biotic, abiotic interfaces that do not degrade over time for high-impact applications, such as functional prosthetics and diabetes management.

### *2.3. Medical Imaging*

High-impact research opportunities in medical imaging fall into two areas. One area is high-resolution in vivo imaging of small populations and clusters of cells or even within a single cell. The second area is portable and affordable imaging systems that can be operated outside the clinical setting, including remote, underserved regions. Wearable electronics, especially cognition monitoring and the gaming industry, are within this category.

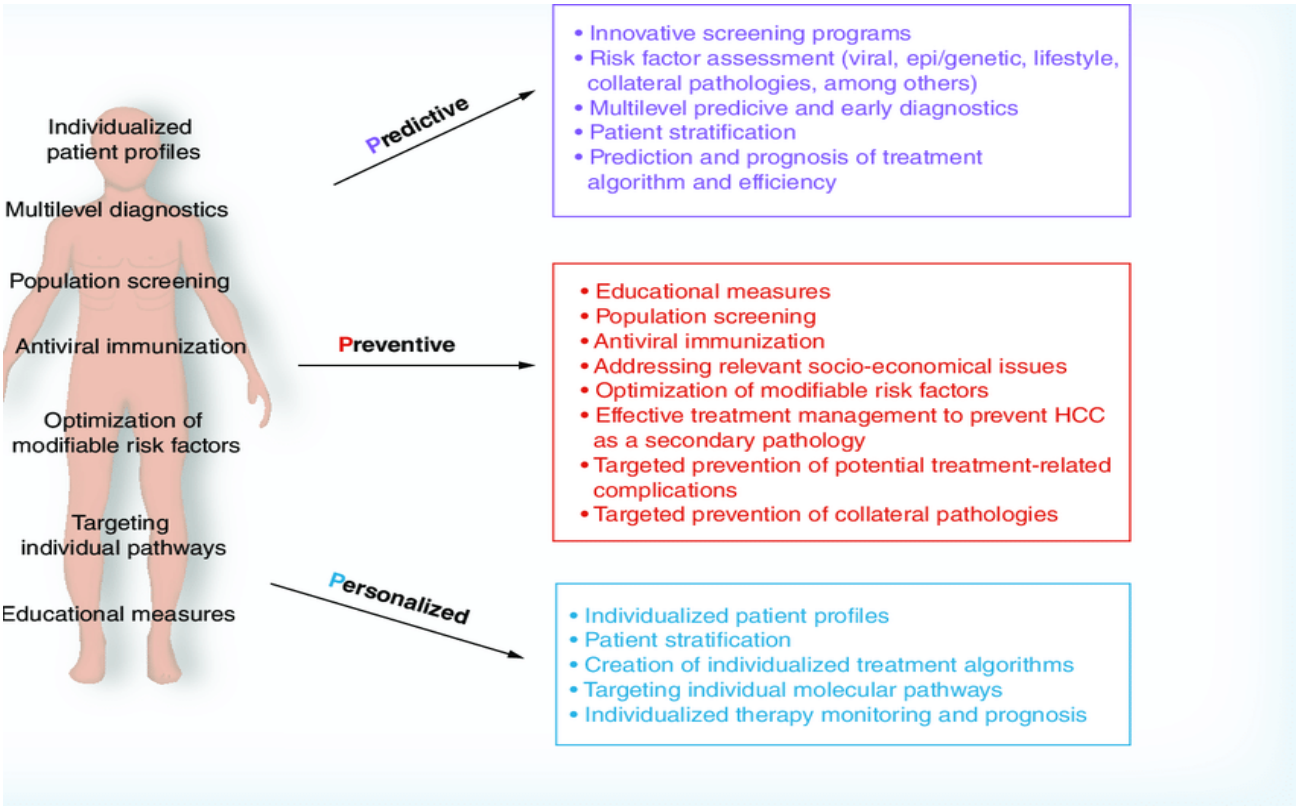


**Fig. 4 Personalized medical diagnostics and monitoring systems[5]**

### *2.4. Recognition of Daily Human Activities Observation*

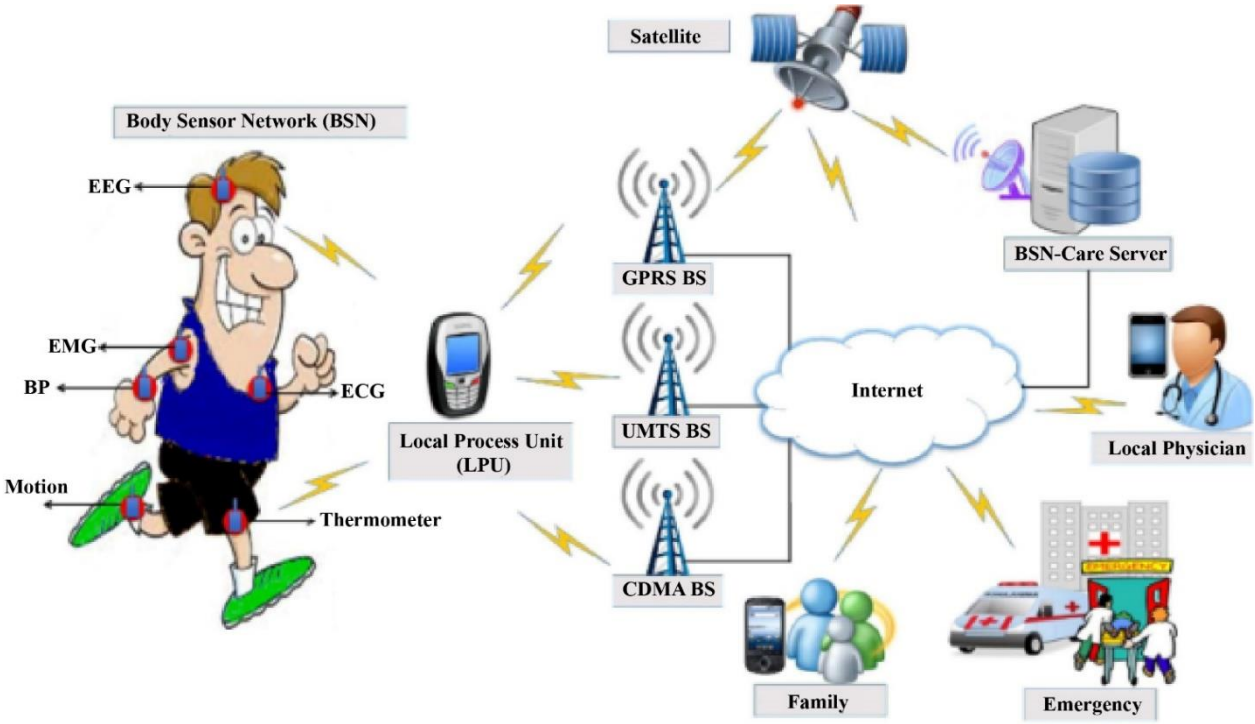


**Fig. 5a Recognition of Daily human activities observation[6]**

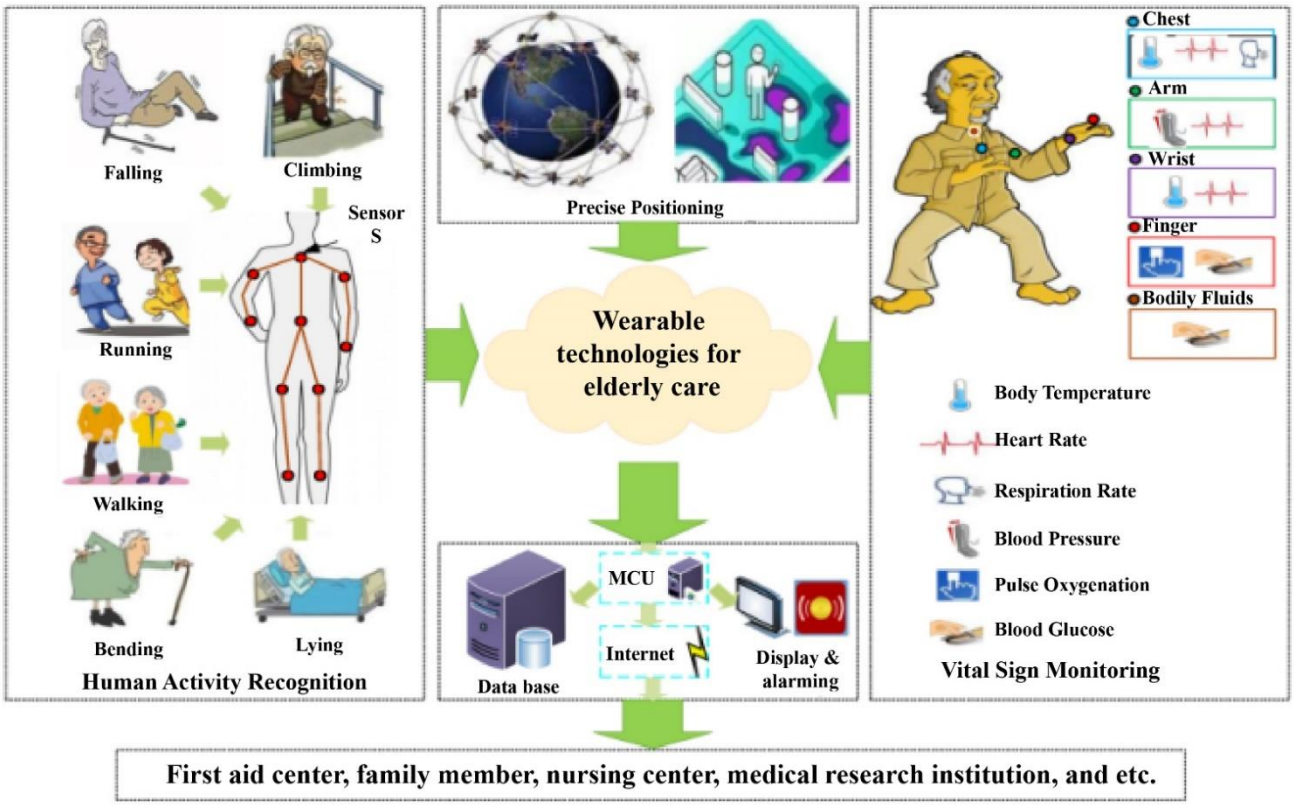


**Fig. 5b Recognition of Daily human activities observation**

## 3. Functions of Polymer-Based Flexible Bioelectronics

Polymer-based bioelectronic devices might integrate various functions, including optical, electrical, and chemical interrogation of neural circuits [4, 5]. Fig.6 shows the functional integration in a fiber-shaped device made by the thermal drawing process and its application to moving mice[6]. Different polymers were designed into fiber-shaped devices with high performance. For instance, PC and COC exhibited low absorptions in the visible spectrum. The differences between their refractive indexes permitted

light confinement within PC, whereas CPE served as a recording electrode. The resulting waveguide, microfluidic channels, and electrodes can be adjusted to allow for simultaneous optical stimulation, drug delivery, and neural recording in behaving mice with high resolution. It further offered more than two months of optogenetic stimulation and drug perturbation.

Fig.6 shows the Performance characterization of polymer-based bioelectronics. Representative illustration of compliant (a)–(c) and stretchable (d)–(f) bioelectronics. (a) Photograph of the flexible self-powered integrated electronic device wrapped over a spatula rod. (b) Scheme of the detecting mechanism. (c) The application to a rat heart with a typical photograph (top) and output current signal (right). (d) Photographs and structure scheme of the stretchable electrode array. (e) Scheme of the in vivo neural stimulation experiment. (f) The percentage of leg movement percentage concerning the full degree of movement under different stimulation voltages between polymer and metal electrodes with the same exposed area (n = 9). (g), (h) Representative illustration of fiber bioelectronics. (g) Photographs of the preparation and cross-sectional structure of a fiber-shaped probe. (h) Photograph of a transgenic mouse with the implanted probe. (i) Chronic electrophysiological recording after injection of CNQX during optogenetic stimulation (10Hz) for up to two months. Reprinted with permission from Ref.[7] and [8].

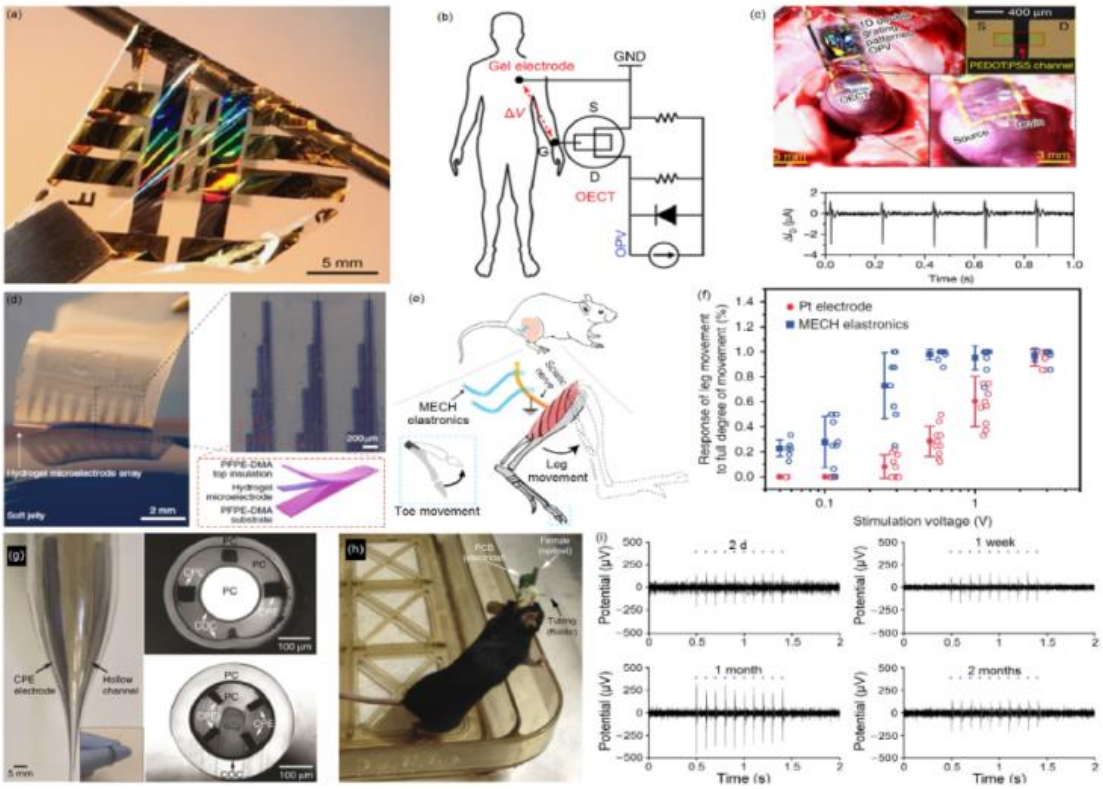


**Fig. 6 Performance characterization of polymer-based bioelectronics**

Assuming that the coils are tuned to the same frequency, the maximum power transmission efficiency for a certain load can be expressed by [9]

$$\eta \frac{1}{1+\frac{1}{k_{12}^2 Q_{PC} Q_{IC}{}_{max}}} \qquad (2)$$

where $k_{12}^2$ , $Q_{PC}$ and $Q_{IC}$ are the coupling coefficient and the quality factors of the unloaded powering coil and the unloaded implant coil, respectively. The maximum power efficiency can be obtained by maximizing the coils' coupling factor and quality factors [10], [11]. To obtain an efficient remote powering link, geometric optimization of the remote powering link is required. However, the dependency of remote powering efficiency on many geometric parameters of the coils, e.g., the number of turns, the width of the conductors and spacing between them, outer and inner diameters, and the coupling between the coils, makes the optimization extremely complicated. The geometric parameters of the coils are swept to obtain the optimal coil pair. The optimized coils' lumped model parameters, shown in Fig. 7, are extracted using analytical equations and field solver software [12], [13]. The remote powering link's power transfer efficiency is calculated using equation(2)[14]. The geometric parameters of the coils are characterized in 3-D electromagnetic field simulation software[15]. Finally, the coils are produced on a printed circuit board (PCB) for reliability, reproducibility, and operation frequency. Fig.8 shows the external link driver. Its output power depends on the supply voltage amplitude, adjusted to deliver the required power level to the implant. A power feedback control controls to supply sufficient power to the implant despite coupling variations continuously.

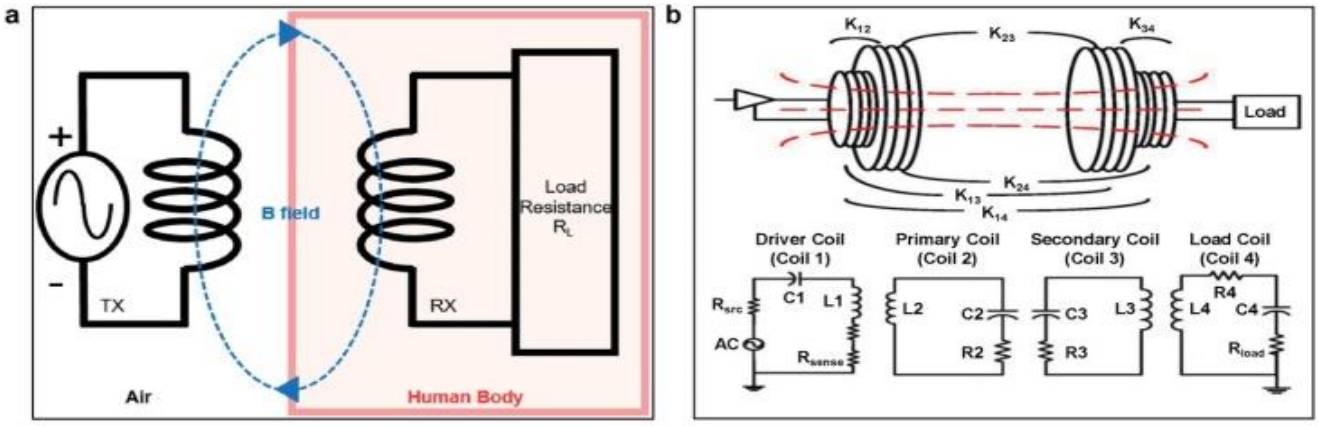


**Fig. 7 Inductive link powering and external link driver[16]**

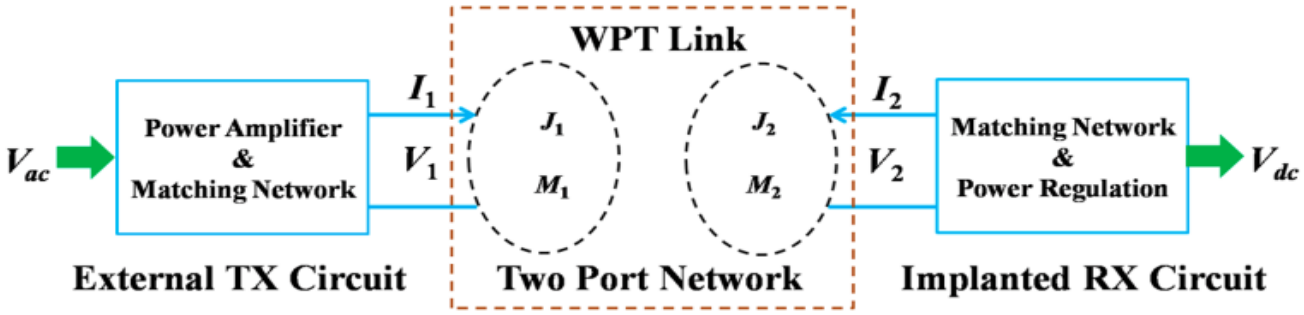


**Fig. 8 Inductive link powering and external link driver[17]**

## 4. Wireless IOT Systems

The Internet of things (IoT) is a key technology and application formed to build a fifth-generation (5G) wireless cellular communication network [18]. 5G connections reached 1 Billion Connections by the end of 2020 and are expected to be 3.5bn by 2026. IOT devices can use 3GPP Cellular wireless access technology as LTE-M and NB-IOT, non-cellular as low-power wide-area (LPWA)as LoRaWAN & Sigfox, and Wi-Fi including the latest Wi-Fi Alliance's Wi-Fi CERTIFIED 6 certification (Wi-Fi 6) which better and more efficient use of the existing radiofrequency. Intel has announced 100s of new Wi-Fi products Industry analysts all agree that the Wi-Fi 6 technology growth will be fast and furious. Several analysts predict that 1 billion Wi-Fi 6 chipsets will ship annually by 2022 [19]. Integration of IoT with Healthcare started with smartwatches monitoring some signals and storing this data in the cloud. With 5G and Wi-Fi 6 networks accelerating the internet connection speeds, and at the same time, Artificial Intelligence offering better analytics tools, sensors technological improvements, more companies in the market are launching new IoT products, including healthcare IoT products[20].

The Medical Device Radiocommunications Service (MedRadio) is a specification and communication spectrum created for and set aside by the US Federal Communications Commission (FCC) for the communication needs of diagnostic and therapeutic medical implants and body-worn medical devices. Devices operating on MedRadio include cardiac pacemakers, defibrillators, neuromuscular stimulators, and drug delivery systems[21].

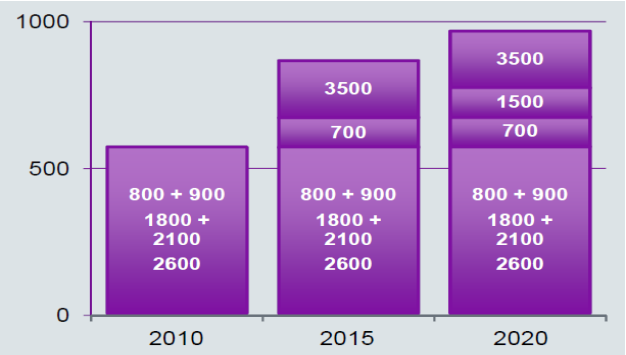


**Fig. 9 WRC approved band by 2020[22]**

**Table.1 shows the frequency band and technology used for Cellular and Wi-Fi 6**

| **Technology** | ***Bands in Mhz*** |
|---|---|
| 2G | 850 / 900 / 1800 / 1900 |
| 3G | 850 / 900 / 1900 / 2100 |
| 4G | 800 / 850 / 900 / 1800 / 2100 / 2600 |
| 5G | 700/900/1800/2100/2600/3500/24000 /26000/28000/37000/39000/47000 upto 90000 |
| WIFI | 2400, 5000,6000 |

As of February 2016, the communications spectrum for these and other similar devices is set aside at various points in the 400 MHz frequency band and the 2360-2400

MHz band, though specifically for medical body area network (MBAN) devices. The specification supersedes and incorporates a previous medical Implant Communication Service (MICS) specification. The specification and nearly identical spectrum have also been created by the European Telecommunications Standards Institute (ETSI), with the specification largely referred to as MICS/MEDS (Medical Data Service) in Europe and other parts of the world[23][24].

## 5. Proposed Embedded Electronics for Inductive Link Powering For IMD

The remotely powered systems consist of two parts. The external part generates the magnetic field for the implanted system and receives the transmitted data. The internal part creates a supply voltage for the implanted system from the induced current and communicates with the external part. The external unit comprises a link driver, a receiver, a supply controller, and a powering coil. Due to the high drain efficiency, the external link driver is chosen as a Class-AB power amplifier to drive the powering coil. Fig.10 shows the inductive link powering and external link driver of the remote powering link. The link is presented by $L_{PC}$ $L_{IC}$M, the powering and implant coils, and mutual inductance, respectively. The $C_{res1}$ $C_{res2}$ capacitors are used for tuning the coils for operation frequency. In addition, $R_{Load}$ represents the load of the remote powering link, which is the input resistance of the implanted rectifier. The M1 $L_{Choke}$ and $C_{sh}$ presents the switching transistor of the amplifier, the choke inductor, and the shunt capacitor, respectively. $L_{Choke}$ $C_{sh}$ And values are chosen to maximize the power efficiency of the power amplifier [25]. The operation frequency of the amplifier is fixed to 2.4GHz by an external oscillator circuit. The output power (Pout) delivered to the load seen by PA $R_L$ is proportional to

$$P_{out} \alpha \frac{V_{sup}^2}{R_L} \quad (3)$$

The Class AB amplifier output stage combines the advantages of Class A and Class B amplifiers while minimizing the problems of low efficiency and distortion associated with them. The Class AB Amplifier is a combination of Class A and Class B for small power outputs; the amplifier operates as a class A amplifier but changes to a class B amplifier for larger current outputs. This action is achieved by pre-biasing the two transistors in the amplifier's output stage. Then each transistor will conduct between 180 and 360 of the time depending on the current output and pre-biasing amount. Thus the amplifier output stage operates as a Class AB amplifier. A Class-AB power amplifier amplifies the modulated RF signal and drives the antenna through an integrated matching network. The critical selection is the chosen architecture and bias point. For output power levels of 20 dBm, a linearly amplifying PA biased in Class AB with little distortion losses is a good choice for a one-stage PA design. The next step is to look at the transistor width. The goal of around 25 to 30 % drain efficiency signifies a DC of around 200 mA. This, in turn, leads to a transistor width of 1 mm for a gate bias between 1.1 V and 1.2 V.

The remotely powered systems consist of two parts. The external part generates the magnetic field for the implanted system and receives the transmitted data. The internal part creates a supply voltage for the implanted system from the induced current and communicates with the external part. The external unit comprises a link driver, a receiver, a supply controller, and a powering coil. The external link driver is chosen as the Class-AB power amplifier to drive the powering coil due to the high drain efficiency of Class-AB.

## 6. Proposed CMOS Class AB PA AS the Link Driver for IMD

This section will involve the schematic, the design equations, the Impedance Transformation, and a detailed explanation of the proposed PA design.

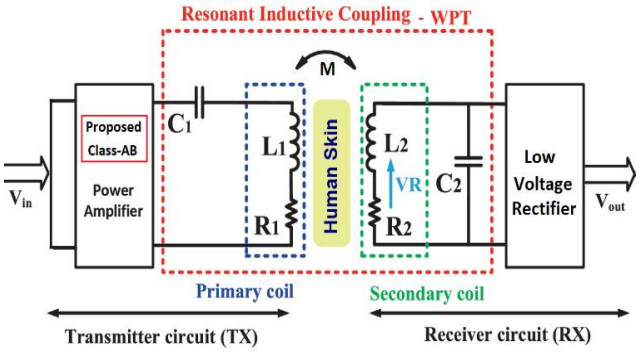


**Fig. 10 Proposed Inductive link powering and external link drive**

### *6.1. Design Optimization of CMOS Class AB PA as link driver for IMD*

Fig.11 shows the schematic of the power amplifier working at a center frequency of 2.4GHz, followed by a 2-section LC matching network to transform the antenna load of 50 Ω to the load of the PA. The matching networks are constructed using the Smith Chart Utility Tool in ADS, as shown in Fig.13. The input matching network is constructed by a 627.547 fF series capacitor, a 4.091 nH shunt inductor, a 1.33 pF series capacitor, and a 33.335 nH series inductor. The output matching network is constructed by a 2.85 nH shunt inductor, a 1.578 pF series capacitor, a 2.107 nH shunt inductor, and a 2.609 pF series capacitor. The matching network's simulated characteristics (S11 and S21) are shown in Fig.13. The transistor sizes of the NMOS are both 100 µm.

The Operation of this CMOS Class AB Power Amp is as follows The RF input is inserted through a port that propagates through the input matching network reaching the lower transistor. The signal is amplified through the cascade amplifier, reaching the output-matching network. The resistances connected to the DC voltages isolate the RF signal from the DC bias.

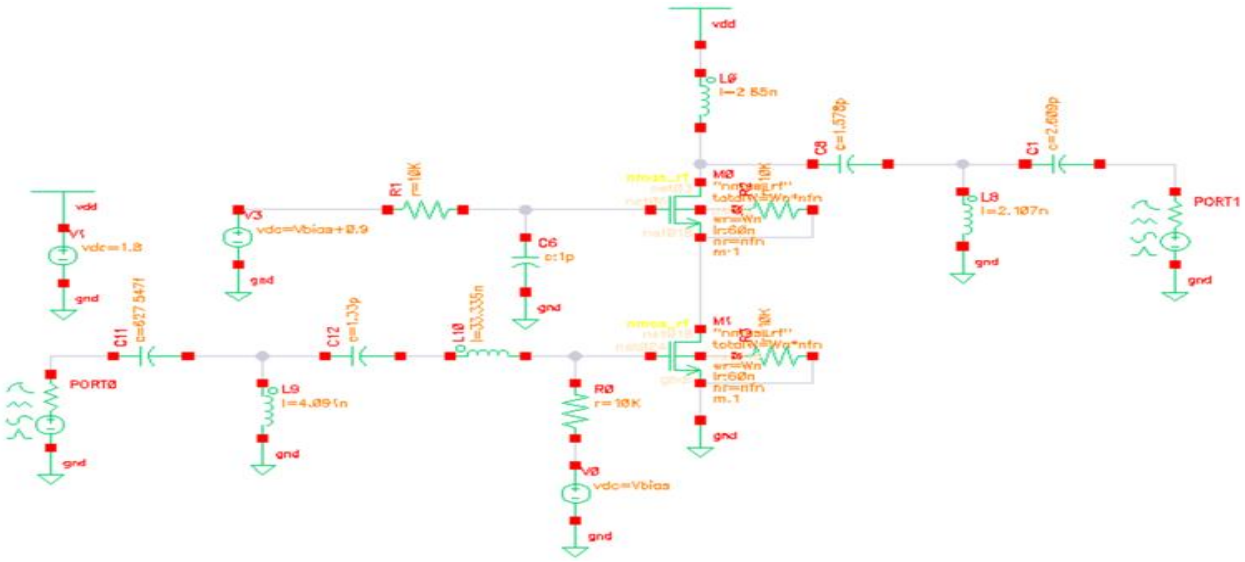


**Fig. 11 Schematic View of CMOS Class AB Power Amp.**

The resistances connected to the bulk and source of transistors are used to reduce the parasitics. Also, the capacitor in the gate of the cascode transistor is used to divide the swing of the signal equally on the two transistors.

### *6.2. Calculated Results*

For the transistor used in simulations, the optimum current density equals 0.7 mA/µm. We choose a maximum theoretical power = 20 dBm. VDD = 1.8 V. So, $10^{20/10}$ x $10^{-3}$ = VDD x Imax. Then Imax = 55.55 mA. We take a margin, so the current is 65 mA.

The optimum output resistance giving the maximum power = $\frac{VDD}{Imax} = \frac{1.8}{65m} = 27.69\ \Omega = 28\ \Omega$.

Jopt = 0.7 mA/µm = $\frac{65m}{W}$ → W = 92.85 µm. We choose W = 100 µm. We choose the biasing voltage that gives this current. Vbias = 850 mV. So the biasing voltage for the cascode transistor = 0.850 + 0.9 = 1.75 V.

The smith chart utility tool existing in ADS software was used to obtain the values of the inductors and capacitors in both the input and output matching networks. It works by putting two dots of the source impedance and the load impedance, which we want to match. The network schematic in Fig.11 represents the matching network required to insert to match along with the values of the inductors and capacitances in it. The matching is made manually on the smith chart, trying to connect the two dots. The software computes the values of the capacitors and inductors.

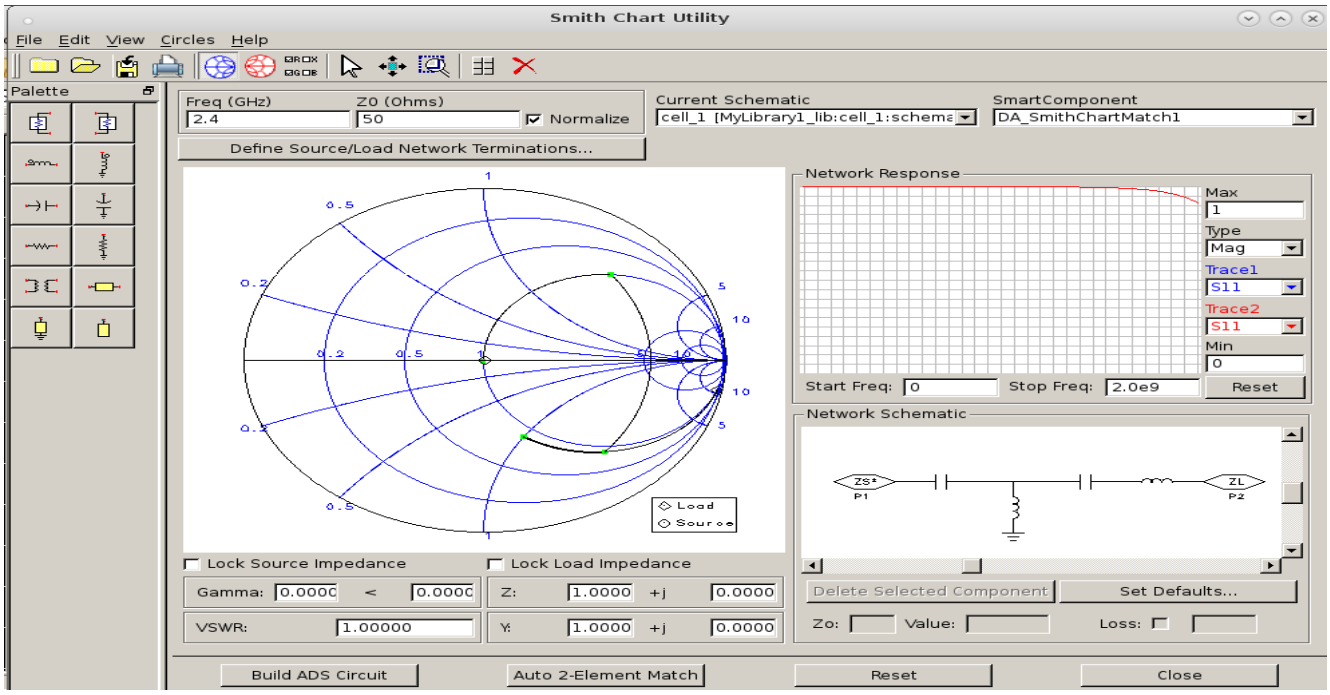


**Fig. 12 Smith Chart Utility Tool**

### *6.3. Simulated Results S- parameters S11 and S21 of Class-AB Power Amplifier*

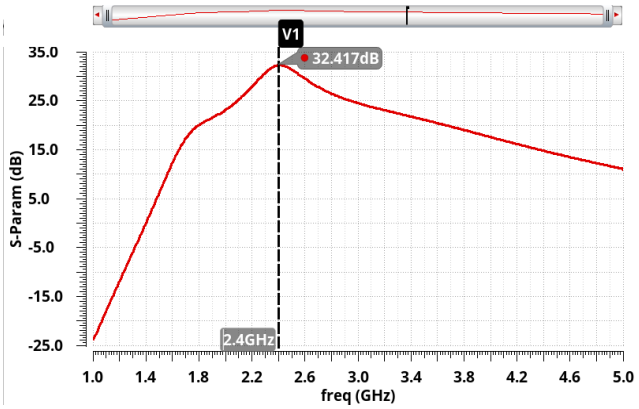


**Fig. 13 Voltage Gain S21= 32.417 dB at F = 2.4 GHz**

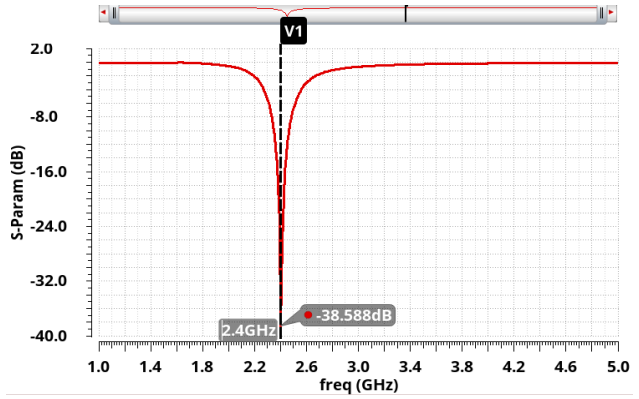


**Fig. 14 Input Reflection Coefficient S11=-38.588 dB**

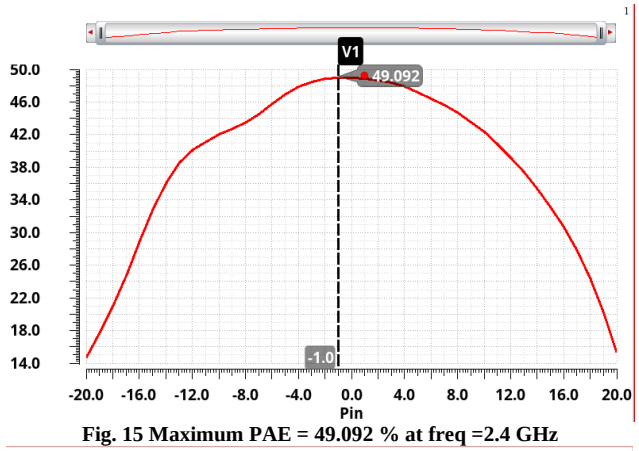


**Fig. 15 Maximum PAE = 49.092 % at freq =2.4 GHz**

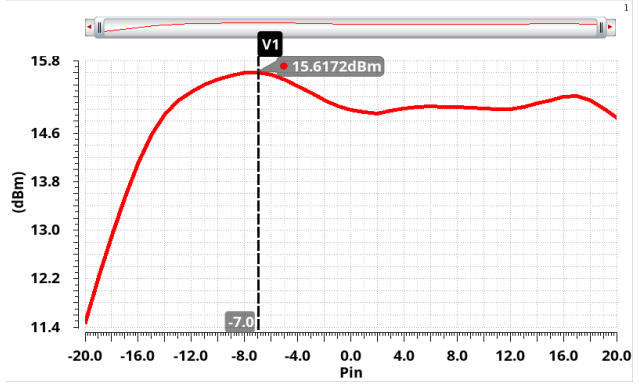


**Fig. 16 Psat = 15.6172 dBm at freq = 2.4 GHz (maximum power got from Pout vs Pin)**

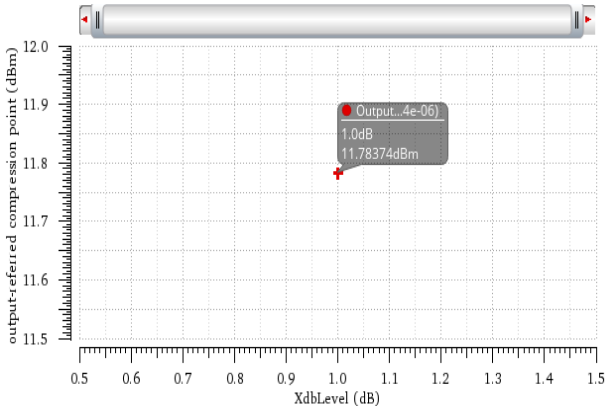


**Fig. 17 P1dB = 11.784 dBm at F = 2.4 GHz**

Performance summary of CMOS Class-AB PA at Freq = 2.4 GHz: Voltage Gain=32.417 dB, Input Reflection Coefficient = -38.588 dB, Power Added Efficiency PAE = 49.092 %, Psat = 15.6172 dBm (maximum power got from Pout vs Pin curve) and P1dB = 11.784 dBm. P1dB: Output referred compression point. The respective physical layout of the CMOS rectifier is presented in Fig. 18.

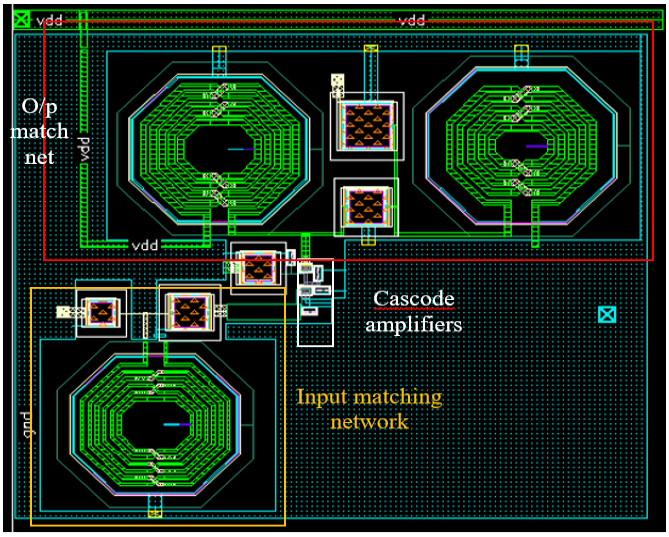


**Fig. 18 Physical layout of the proposed CMOS rectifier**

The proposed rectifier layout has a 0.085mm2 chip area, as shown in Fig.18.

## 7. Conclusion

The paper presents remote powering for implantable medical devices and different sensor/actuator networks. A permanently implanted device is placed under the skin and stores the measured data. A mobile external unit charges the implanted device and receives the data from the implant. A Class-AB Power Amplifier is proposed to improve the efficiency of the efficient power transfer. The power required by implantable electronics, including the one for wireless communication, is 0.6 mW. In this paper, methodologies to transfer and harvest energy in implantable medical devices are introduced and discussed to highlight the uses and significance of various potential power sources, followed by in-depth discussions of the most popular method, namely inductive linking. The circuits

have been designed and simulated in tsmc 65nm CMOS technology. The circuit simulations were done using CADENCE Design Tools to optimize the design and get the required specifications for the proposed system. The power amplifier's operating class is generally based on linearity and power efficiency requirements.

For applications in which linearity is a critical issue. In contrast, good efficiency is desired; a linear-mode amplifier, e.g., Class AB, is suitable with a simple topology, leading to optimal production and system operation costs. So, In this paper, a 2.4 GHz Class AB CMOS PA with CG driver stage followed by CS power stage was designed using the proposed method for WBAN applications. The simulation results showed that the proposed PA achieved a maximum PAE of 49.09% and had an average gain of 32.4 dB over the frequency of interest in Industrial, Scientific, and Medical (ISM) bands. Input Reflection Coefficient S11=-38.588 dB. Psat=15.6172 dBm Output referred compression point P1dB=11.784 dBm. The Physical layout of the proposed CMOS Class-AB Amplifier has been designed and optimized to a 0.085mm$^2$ chip area.

## References


[1] George D. Spyropoulos et al., "Mixed-Conducting Particulate Composites for Soft Electronics," *Science Advances*, vol. 6, no. 17, 2020. *Crossref,* http://doi.org/10.1126/sciadv.aaz6767

[2] Eleonora Macchia et al., "About the Amplification Factors in Organic Bioelectronic Sensors," *The Royal Society of Chemistry*, vol. 7, pp. 999-1013, 2020. *Crossref,* http://doi.org/10.1039/c9mh01544b

[3] Ariana Villarroel Marquez, Niall McEvoy, and Amir Pakdel, "Organic Electrochemical Transistors (OECTs) toward Flexible and Wearable Bioelectronics," *Journal of Molecules, Department of Mechanical, Manufacturing & Biomedical Engineering*, vol. 25, no. 22, p. 5288, 2020. *Crossref,* https://doi.org/10.3390/molecules25225288

[4] Meenakshi et al., "Switchable Graphene-Based Bioelectronics Interfaces," *Chemosensors*, vol. 8, no. 2, pp. 45, 2020. *Crossref,* https://doi.org/10.3390/chemosensors8020045

[5] Godspower W. Omokhunu, and Christian Bach, "Organic Bio-Electronics: Bridging the Gap Between Natural and Artificial Materials for Bio-Electronics," *EJERS European Journal of Engineering Research and Science*, vol. 4, no. 1, pp. 85-91, 2019. *Crossref,* https://doi.org/10.24018/ejers.2019.4.1.635

[6] Krishna Feron et al., "Organic Bioelectronics: Materials and Biocompatibility," *International Journal of Molecular Sciences*, License CC BY, vol. 19, no. 8, pp. 2382, 2018. *Crossref,* https://doi.org/10.3390/ijms19082382

[7] Hyun SeokSong et al., "3D Hydrogel Scaffold Doped with 2D Graphene Materials for Biosensors and Bioelectronics," *Biosensors and Bioelectronics*, vol. 89, no. 1, pp. 187-200, 2017. *Crossref,* https://doi.org/10.1016/j.bios.2016.03.045

[8] Yoichi Aoki, "Photovoltaic Performance of Organic Photovoltaics for Indoor Energy Harvester," *Organic Electronics*, vol. 48, no. c, pp. 194-197, 2017. *Crossref,* https://doi.org/10.1016/j.orgel.2017.05.023

[9] D. R. Cox et al., Organic Photovoltaic Cells: Heliatek Claims Conversion Efficiency Record by Nancy Owano TechXplore.com, Statistical Thinking for 21st-Century Scientists, *Science Advances*, 2017.

[10] Seth R Marder, and Jean-Luc Bredas, "*The WSPC Reference on Organic Electronics: Organic Semiconductors, Fundamental Aspects of Materials and Applications,*" Saudi Arabia & Georgia Institute of Technology, King Abdullah University of Science & Technology, USA, vol. 2, no. 2, 2016. *Crossref,* https://doi.org/10.1142/9678.

[11] Srilalitha, Jayaveera, and Madhvendhra, "The Effect of Dopant, Temperature, and Band Gap on Conductivity of Conducting Polymers," *International Journal of Innovative Research in Science, Engineering and Technology*, vol. 2, no. 7, 2013.

[12] Kareema Majeed Ziadan, *Conducting Polymers Application*, New Polymers for Special Application, Intech, 2012.

[13] Susanne Löffler, Ben Libberton, and Agneta Richter-Dahlfors, "Organic Bioelectronic Tools for Biomedical Applications," *Electronics*, vol. 4, no. 4, pp. 879-908, 2015. *Crossref,* https://doi.org/10.3390/electronics4040879

[14] Alwin Ming-Doug Wan et al., "3D Conducting Polymer Platforms for Electrical Control of Protein Conformation and Cellular Functions," *Journal of Materials Chemistry B*, vol. 3, pp. 5040-5048, 2015. *Crossref,* https://doi.org/10.1039/C5TB00390C

[15] Mawad D, Lauto A, and Wallace G.G, "*Polymeric Hydrogels as Smart Biomaterials,*" Kalia, S., Ed., Springer Series on Polymer and Composite Materials; Springer: Cham, Switzerland, 2016.

[16] Mohammad Javadi et al., "Conductive Tough Hydrogel for Bioapplications," *Macromolecular Bioscience*, vol. 18, no. 2, 2017. *Crossref,* https://doi.org/10.1002/mabi.201700270

[17] G.L.Mario Cheong et al., "Conductive Hydrogels with Tailored Bioactivity for Implantable Electrode Coatings," *Acta Biomaterials*, vol. 10, no. 3, pp. 1216-1226, 2014. *Crossref,* https://doi.org/10.1016/j.actbio.2013.12.032

[18] Anton Mihic et al., "A Conductive Polymer Hydrogel Supports Electrical Cell Signaling and Improves Cardiac Function After Implantation Into a Myocardial Infarct," *Circulation*, vol. 132, no. 8, pp. 772-784, 2015. *Crossref,* https://doi.org/10.1161/CIRCULATIONAHA.114.014937

[19] Josef Goding et al., "A Living Electrode Construct for Incorporating Cells Into Bionic Devices," *MRS Communication*, vol. 7, no. 3, pp. 487-495, 2017. *Crossref,* https://doi.org/10.1557/mrc.2017.44

[20] Baolin Guo, Lidija Glavas, and Ann-Christine Albertsson, "Biodegradable and Electrically Conducting Polymers for Biomedical Applications," *Progress in Polymer Science*, vol. 38, no. 9, pp. 1263-1286, 2013. *Crossref,* https://doi.org/10.1016/j.progpolymsci.2013.06.003Get rights and content

[21] Amin S. Ibrahim et al., "Traffic Modeling of Smart City Internet of Things Architecture," *IET Communication*, vol. 14, no. 8, pp. 1275-1284, 2020. *Crossref*, https://doi.org/10.1049/iet-com.2019.1252

[22] Ericsson Mobility Report, 2021. [Online]. Available: https://www.ericsson.com/en/reports-and-papers/mobility-report/reports/november-2021

[23] [Online]. Available: https://www.extremenetworks.com/wifi6/what-is-80211ax/

[24] "*ITU Radio Regulations Articles*," Edition, 2020.

[25] "Technology Strategic Guidance Spectrum Optimization," VEON Group, 2013.